# Response Characteristics of Zone Resistance in Aluminium Reduction Cell

**Chun Li[1], Jun Tie[2], Yi Meng[3], Hao Xiao[4], Jun Lei[5], Dongwei Liu[6] and Boyang Liu[7]**
1. Lecturer
2. Professor
3. Associate Professor
North China University of Technology, Beijing, China
4, 5, 6, 7. Process Engineer
Beijing SWT Intelligent Optics Technology, Beijing, China
Corresponding author: tiejun67@263.net
https://doi.org/10.71659/icsoba2024-al033

**Abstract**

The aluminium reduction cells can be segmented into several relatively individual zones surrounding the feeders, but the current alumina feeding system still mostly has multiple feeding points to perform simultaneous operations or two groups of feeding points to perform alternately operations, which often results in high or low alumina concentration in certain zones of the cell, leading to faults such as low-voltage anode effects and cell bottom sludge, reducing the current efficiency. The optical fibre current sensor can accurately measure the zone current and individual anode current online, providing conditions for localized independent feeding control method. Zone currents in a 400 kA cell were continuously monitored in this study. The varying characteristics of the resistance in each zone and the cell resistance were analysed. The results indicate that the zone resistance exhibits greater sensitivity to changes in alumina concentration than the cell resistance. Therefore, this paper presents a preliminary method that can either optimize the existing simultaneous feeding control or achieve localized independent feeding control based on the zone resistances obtained from the accurate measurements of zone currents and individual anode currents.

**Keywords:** Aluminum electrolysis, Optical fiber current sensor, Zone resistance, Localized independent feeding control.

## 1. Introduction

Prebaked anode aluminum reduction cells contain dozens of anodes. For example, 400 kA and 500 kA electrolytic cells have 48 anodes, while 600 kA electrolytic cells have as many as 56 anodes. These anodes are connected in parallel and collectively carry the electrolysis potline current flowing through the electrolytic cell. Although the potline current has been accurately measured nowadays, the precise value of the current carried by each individual anode remains a great challenge.

The online measurement of individual anode currents was first conducted in the 1970s by Reynolds Metals Company, aiming to detect anode spikes and instabilities. Subsequently, Alcoa also performed measurements of single anode currents and utilized them for independent control experiments during the production process [1]. They adopted the voltage drop method, which involves estimating current by measuring the voltage drop generated by the current flowing through a conductor. This method, known for its simplicity, ease of implementation, and cost-effectiveness, remains widely used in production site research even today. Over time, the measurement positions have shifted from the initial anode rods to the side [2] and top [3] of the anode beam, while the underlying measurement principle remained unchanged. Evans et al. [4] introduced the "many sensors method", employing a sufficient number of Hall sensors to de-

convolute the anode current on the anode beam by minimizing interference from the electrolytic cell's background magnetic field. They conducted extensive industrial application tests over several years to monitor changes in anode current [5-7].

The fiber-optic current sensing measurement technology, based on the Faraday magneto-optic effect and Ampere's circuital law, can theoretically eliminate the influence of background magnetic fields and offers high precision. It has now replaced traditional Hall sensors as the primary method for measuring electrolysis potline currents [8]. Our team has taken the lead in conducting experiments using optic fiber current sensors to measure anode currents in aluminum electrolytic cells, verifying the accuracy of measurements of anode currents, pillar busbar currents, and cathode currents [9]. Potocnik et al. [10] subsequently reported similar measurements and compared the high precision characteristics of optic fiber current sensors with other measurement methods. However, due to the inherently high cost of optic fiber current sensors, they have not been used for online measurement of anode currents in electrolytic cells.

Considering the fact of uneven alumina concentration distribution in large aluminum electrolytic cells, independent feeding control for each zone has the potential to significantly improve the uniformity of alumina concentration in the electrolytic cell and greatly enhance electrolysis efficiency [11]. Based on our scheme for measuring individual anode currents using optical fiber sensors [12], we propose a method using 5 or 3 optical fiber loops to measure zone anode currents [13]. Furthermore, we introduce a method utilizing a saddle-shaped optical fiber loop to measure zone anode currents with just one optical fiber loop [14, 15]. Taking an electrolytic cell with 48 anodes and 6 feeding zones as an example, the number of sensors required for measuring zone anode currents is reduced from 48 to 16, 11, or 6, depending on whether 5, 3, or 1 optical fiber loop(s) measurement schemes are used, respectively. Based on an assessment of the benefits achieved, this approach has become economically acceptable for electrolytic workshops.

This paper reports the measurement results conducted by our team on a 400 kA electrolytic cell using a “5 optical fiber loops measurement scheme”. The characteristics of zone current changes and the feasibility of localized independent feeding control based on zone current have been discussed. In addition, the response characteristics of zone currents to anode effects have also been monitored in this study.

## 2. Experimental Measurement of Zone Currents

The measurement experiments were conducted on a 400 kA electrolytic cell at a specific enterprise. This electrolytic cell underwent major repairs in 2023 and uses a graphitized cathode. It also served as a test cell for low-voltage electrolysis at this enterprise. The electrolytic cell featured 48 anodes and 6 feeders, with each feeder supplying alumina to the surrounding 8 anodes. The alumina feeding control strategy is to alternate underfeed and overfeed, and the feeding speed is equal in 6 zones. The cell voltage is approximately 3.81 V.

In late September 2023, our team installed 6 sensing optical fiber loops on the pillar busbars of the electrolytic cell for online measurement of pillar busbar currents. Simultaneously, sensors for measuring currents in two feeding zones were installed on the horizontal busbars, with a sampling interval of 1 second, to verify the feasibility of optical fiber current sensors. By the end of April 2024, based on the preliminary work, all 16 sensing optical fiber loops were installed on the horizontal busbars, enabling online measurement of zone anode currents throughout the entire cell. And the cell voltage information was collected synchronously. Figure 1(a) illustrates the measurement scheme, while Figures 1(b) and (c) show physical photos of the sensors installed on the pillar busbars and horizontal busbars, respectively. Figure 1(d) presents the real-time zone current data displayed on the industrial control computer used for measurement.

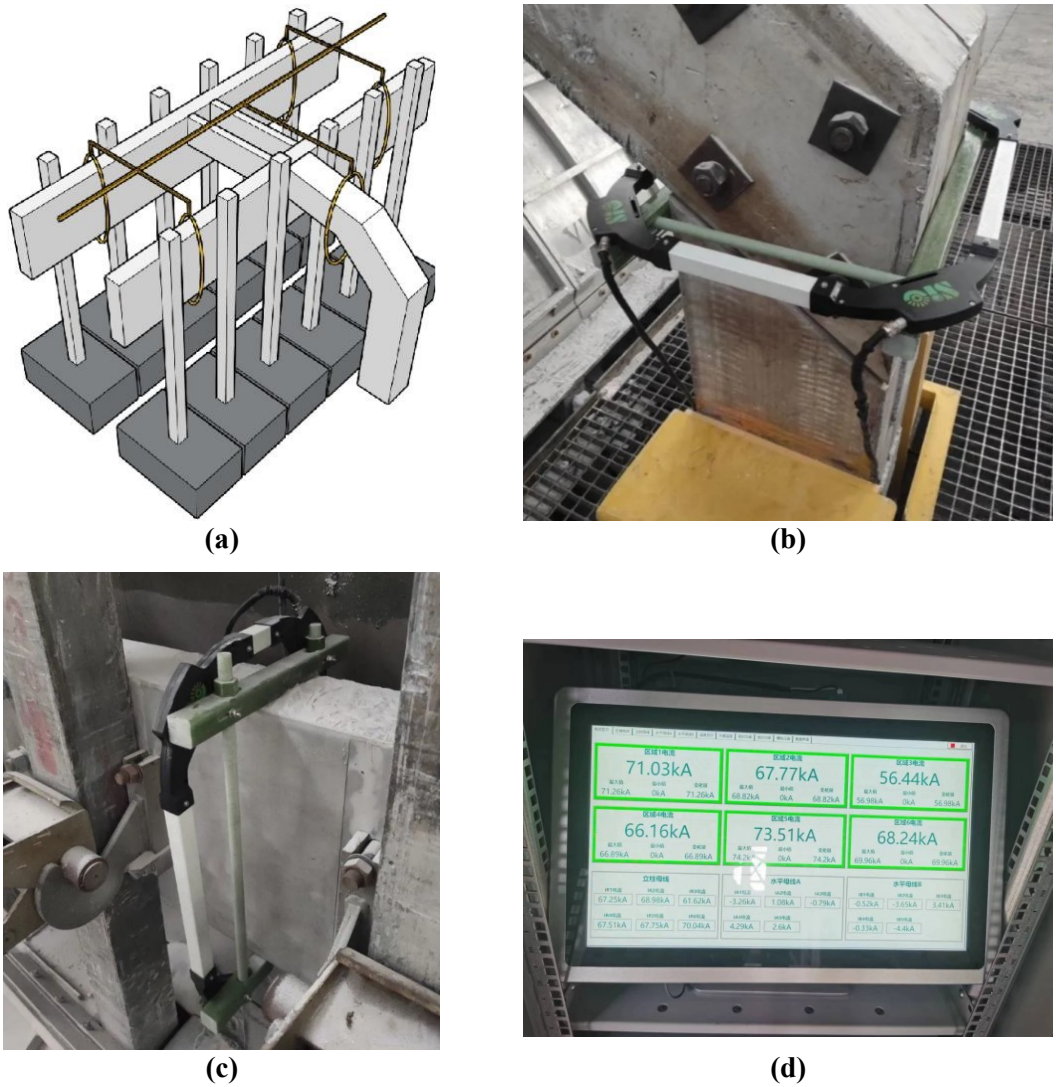


**(a)** **(b)**

**(c)** **(d)**

**Figure 1. The measurement scheme of optical fiber loops installed on the cell (a); The physical photos of the sensors installed on the pillar busbars (b) and horizontal busbars (c); The real-time measurement data (d).**

## 3. Measurement Results and Analysis

Based on six months of measurement data, a comparison between the pillar busbar currents, the sum of zone currents, and the potline current reveals that the deviation between the measured total current and the potline current is less than 2000 A, with a relative deviation of less than 0.5 %. This accuracy fully meets the requirements of industrial control.

### 3.1 Zone Currents

Figure 2(a) shows the continuous measurement results of total and zone currents over a five-day period from midnight on April 27$^{th}$ to May 1$^{st}$, while Figure 2(b) illustrates the corresponding distribution analysis. Table 1 provides the comparative overview of the average values and variation coefficients of current data. As shown in Figure 2, the measured total current (considered as the potline current) remains remarkably stable at around 402 kA, with the variation coefficient at just 0.12 %. However, the currents in different zones vary significantly, ranging from a minimum of 50 kA to a maximum of 70 kA. Compared to the average, these values deviate by

5 % and 15 %, respectively. The current distribution also differs, with Zone 5 exhibiting the highest variation coefficient at 0.79 % and Zone 1 showing the lowest at 0.5 %. Nevertheless, even the lowest variation is considerably higher than that of the total current, indicating that zone currents are constantly changing despite the stability of the potline current. Indeed, Figure 2(a) clearly demonstrates a steady increase in Zone 5's current and a continuous decrease in Zone 6's current. Additionally, typical step-like decreases in zone currents and corresponding step-like increases in neighboring zones were observed, which are attributed to the current changes resulting from anode-changing operations during the production process.

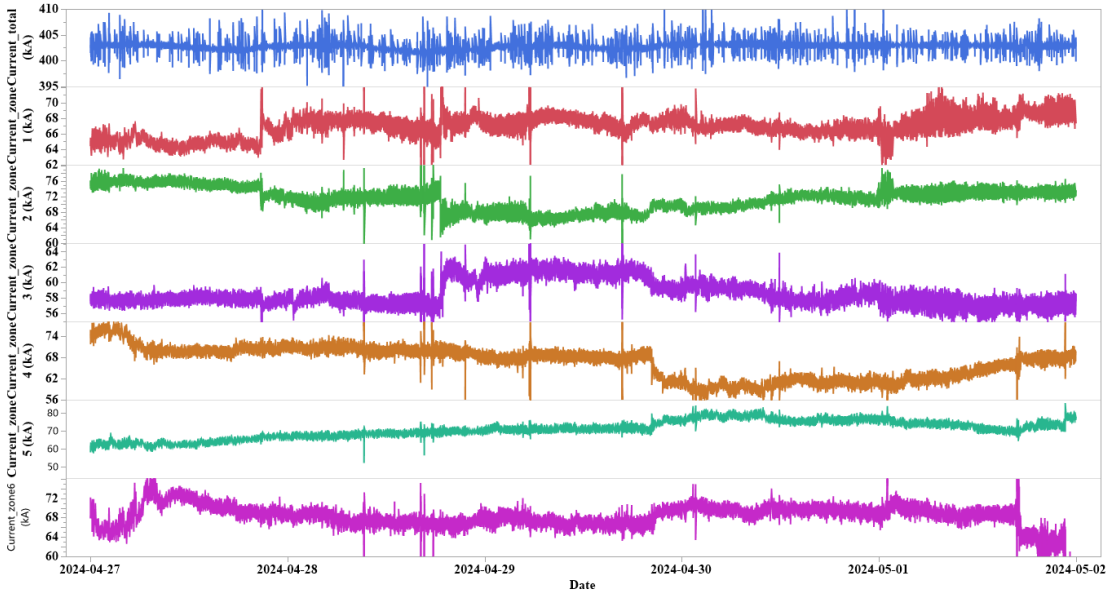


**(a)**

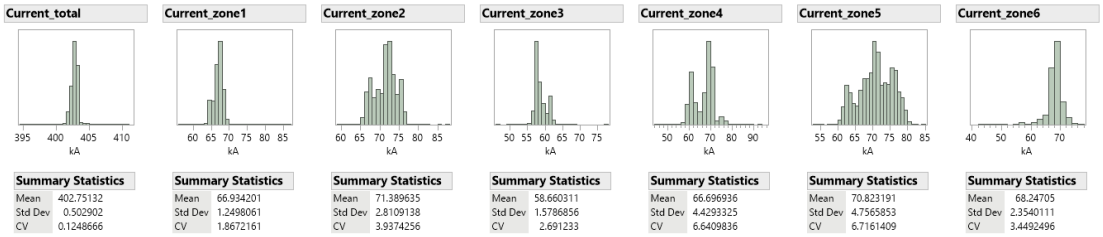


**(b)**

**Figure 2. The continuous measurement results (a) and distribution analysis (b) of total current and different zone currents from midnight on April 27th to May 1st.**

**Table 1. The average values and variation coefficients of the measured current data from midnight on April 27th to May 1st.**

| Current | Zone current | | | Total current |
|---|---|---|---|---|
| | Average | Maximum | Minimum | |
| Average value (kA) | 67 | 71.4 | 58.6 | 402.8 |
| variation coefficient (%) | 4.22 | 6.7 | 1.9 | 0.12 |

Based on Figure 2, it can be concluded that during the production process, the rate of alumina consumption varies across different zones, with deviations of up to 20 % from the average (as seen in the anode effect monitoring curve in Figure 6, where the maximum current differs from

the average by almost 20 %). The synchronous equal-speed feeding operation across six zones currently used is bound to result in excess alumina in some zones and deficiencies in others. This imbalance can lead to low-voltage anode effects or precipitation in certain zones, which are caused by chronic undersupply or incomplete dissolution, respectively. If the feeding rate in each zone were independently controlled based on real-time current, it would significantly reduce the likelihood of feeding process-related issues.

### 3.2 Response Characteristics of Zone Resistances to Feeding Process

Formula (1) gives the definition of cell resistance, which is also used to define the resistance of each zone.

$$R = \frac{V - V_{ext}}{I} \quad (1)$$

where:

$V$ Cell voltage, V
$V_{ext}$ Extrapolated voltage, 1.65 V
$I$ Potline current or zone current, A

Figure 3 illustrates the resistance variation curve corresponding to Figure 2(a). Unlike the stability of the total current, the cell resistance $R\_cell$ shown in Figure 3 exhibits distinct regular fluctuating characteristics. Table 2 lists the characteristic data of resistance fluctuations corresponding to Table 1. It is evident that the variation coefficient of cell resistance is as high as 1.71 %, which is much greater than that of the total current (0.12 %). This indicates that the fluctuations in cell resistance are almost entirely caused by the fluctuations in cell voltage. The zone resistances generally reflect the trend of zone current changes while also showing the characteristics of cell voltage variations. They possess similar fluctuating properties to cell resistance. The average, maximum, and minimum coefficients of variation listed in Table 2 are slightly higher than the corresponding current data items in Table 1, which is clearly due to the contribution of cell voltage variations. Based on the absolute numerical values, for example, the average coefficient of variation for zone current is 4.22 %, while the average for zone resistance is 4.68 %. This suggests that the changes in zone current contribute to nearly 90 % of the variation in zone resistance.

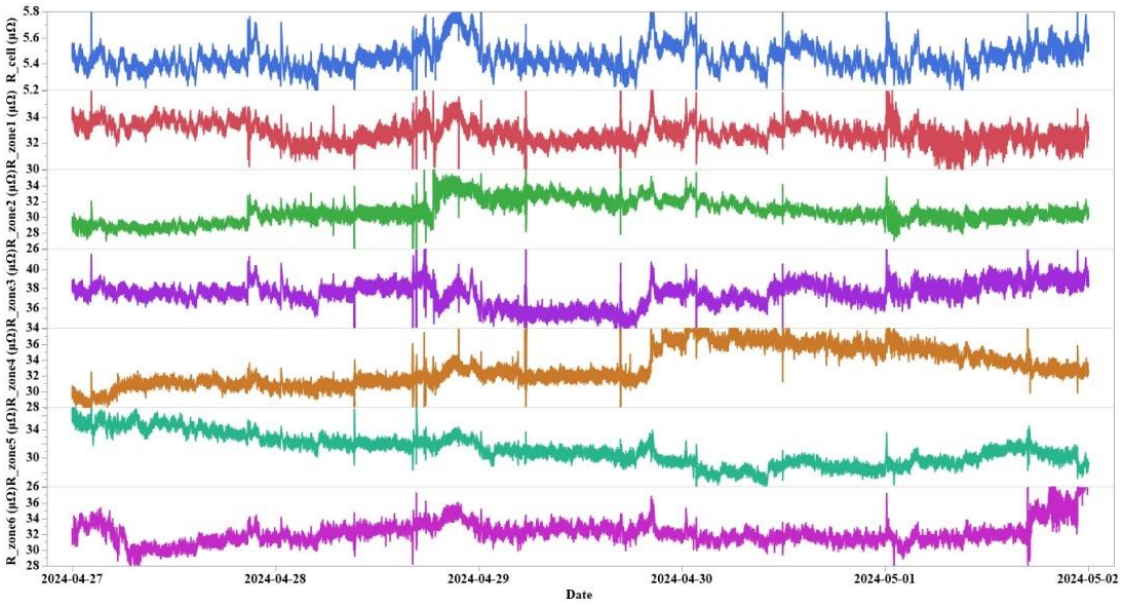


**Figure 3. The variation curve of cell resistance and different zone resistances from midnight on April 27th to May 1st.**

**Table 2. The average values and variation coefficients of the resistance data from midnight on April 27th to May 1st.**

| Resistance | Zone resistance | | | Cell resistance |
|---|---|---|---|---|
| | Average | Maximum | Minimum | |
| Average value (μΩ) | 32.9 | 37.4 | 30.8 | 5.45 |
| variation coefficient (%) | 4.68 | 7.11 | 2.22 | 1.71 |

As is well known, the regular fluctuations in cell resistance are primarily caused by the alternating process of underfeeding and overfeeding in the electrolytic cell. We are also interested in how zone resistances respond to the feeding process. Thus, we analyzed zone resistance data collected during a relatively stable period on April 28th, as illustrated in Figure 4. This figure clearly shows that the fluctuations in cell resistance are highly regular; specifically, the cell resistance increased during underfeeding and decreased during overfeeding. The zone resistances exhibit similar characteristics, with the zone resistance increasing during underfeeding and decreasing during overfeeding. However, the magnitude of these changes is greater than that of the cell resistance, and the variations differ across zones.

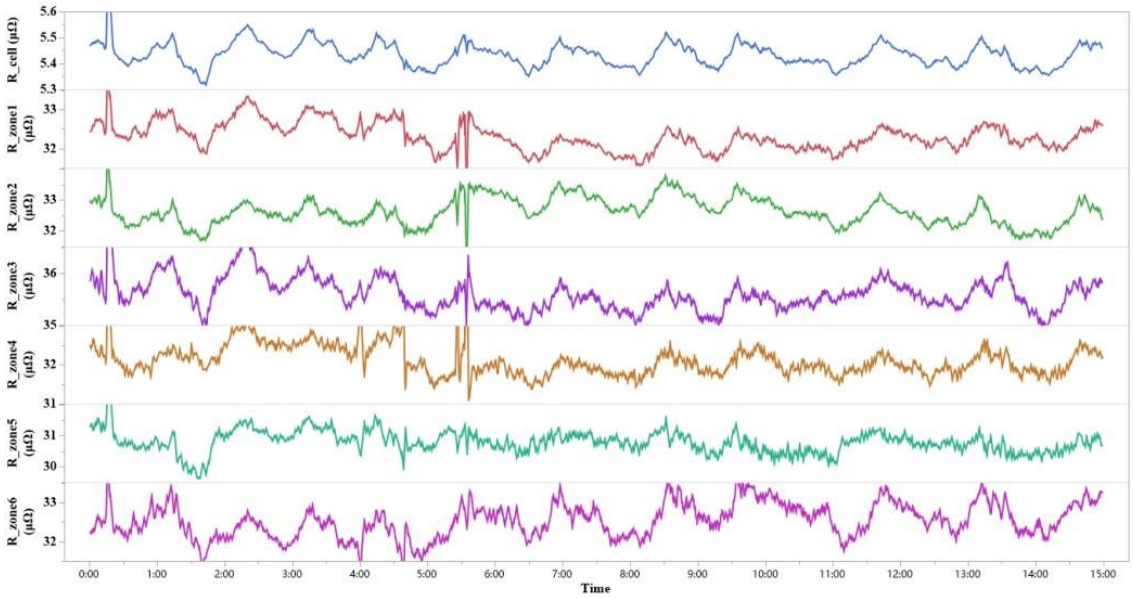


**Figure 4. The response of zone resistance curves to the feeding process (the zone resistance data collected during a relatively stable period on April 28th).**

Figure 4 suggests that independent control of feeding in each zone can be achieved by referencing the existing feeding control method for the entire cell. This would require modifications to the existing feeding (crust breaking) system. If the electrolytic cell control system lacks independent control functionality, the existing control strategy can be collaboratively optimized based on the variation characteristics of zone resistances. For instance, by monitoring changes in zone resistances in real-time, the upper and lower limits of zone resistance variations can be used as a basis for switching feeding schedules, alongside the upper and lower limits of cell resistance variations. This approach can prevent individual zones from exceeding the upper and lower limits of alumina concentration, further improving the uniformity of alumina concentration.

### 3.3 Response of Zone Currents and Resistances to Anode-changing Operations

Figure 5 illustrates the response of zone currents and resistances during two typical anode-changing operations. Figure 5(a) shows the replacement of A7 and A8 anodes in Zone 2 on April 28th. It can be seen that during the anode change, the current in the anode-changing zone dropped stepwise from 73 kA to 66 kA and stabilized, causing a transient increase in zone 1's current from 66 kA to 72 kA, followed by a decrease to 68kA. However, the current in Zone 3 increased by 5 kA in a more complex manner. Since the increased currents in Zones 1 and 3 fully absorbed the decreased current in Zone 2, there were no significant changes in the currents of Zones 4, 5, and 6, hence they are not shown in the figure. Changes in zone resistances are exactly opposite to the increases or decreases in zone currents. The resistance in the anode-changing zone increases, while the resistances in adjacent zones decrease. This is a result of the definition in Formula (1). Additionally, since resistance changes also depend on cell voltage, the pattern of these changes is not entirely determined by current.

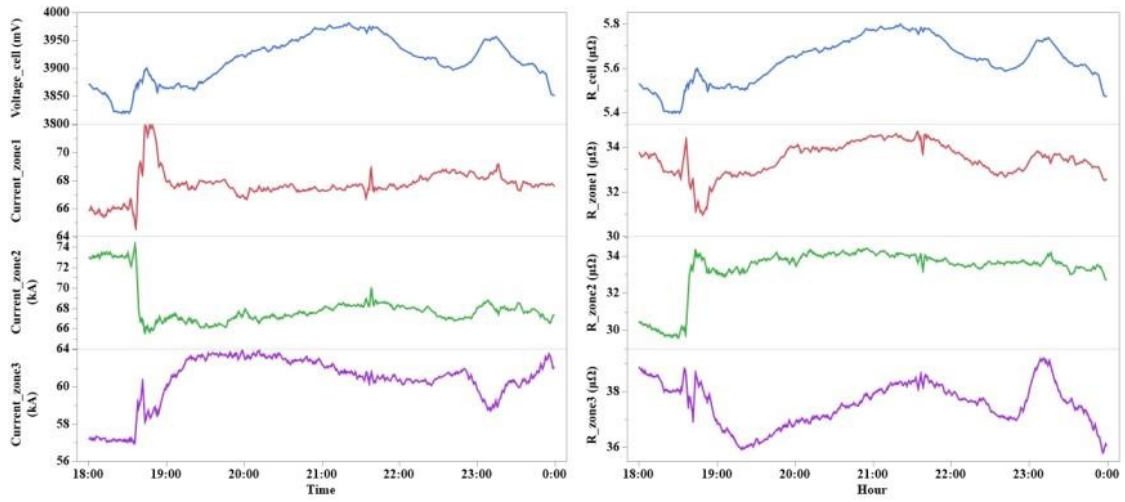


**(a)**

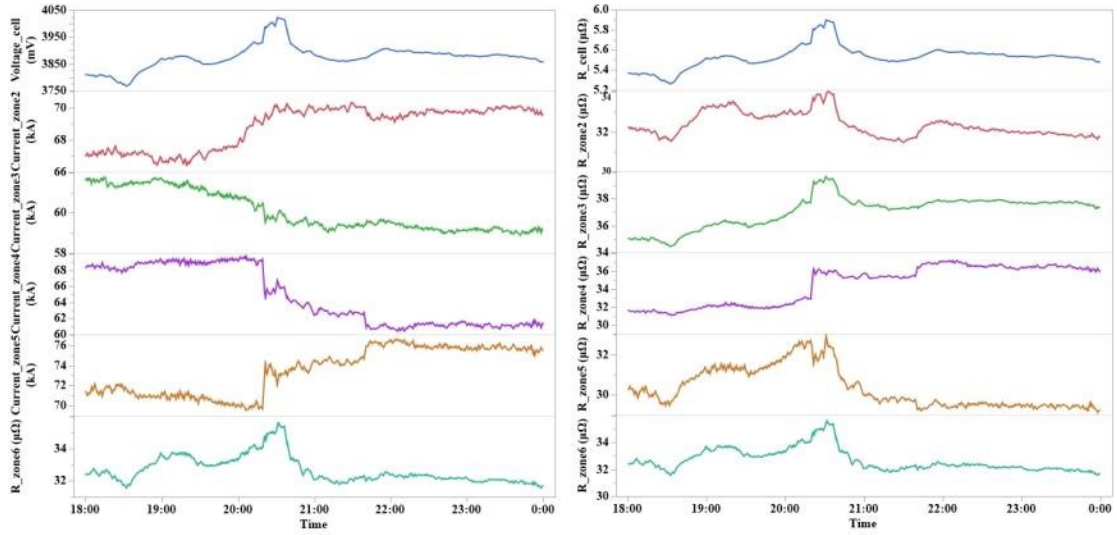


**(b)**

**Figure 5. The response of cell voltage, zone currents and resistances during two typical anode-changing operations. (a) the replacement of A7 and A8 anodes in Zone 2 on April 28th, (b) the replacement of B15 and B16 anodes in Zone 4 on April 29th.**

Unlike Figure 5(a), Figure 5(b) illustrates the replacement of B15 and B16 anodes in Zone 4 on April 29th. In this case, the adjacent Zone 3's current seemed unaffected and did not increase but rather continued to decrease gradually. On the other hand, Zone 5 on the other side appeared to fully absorb the decreased current from Zone 4, increasing in a nearly symmetrical pattern with Zone 4. It can be observed that the changes in Zone 2 and Zone 3 were almost symmetrical, while the current in Zone 6 also seemed to be influenced by the aforementioned zones. Evidently, the impact of anode-changing operations mainly occurred in adjacent zones, but not necessarily affecting both neighboring zones. Since the replaced B15 and B16 anodes were closer to Zone 5, it is understandable that Zone 5 was significantly affected.

Upon observing Figure 5, it is also noticeable that anode-changing operations have a significant impact on cell voltage, adding complexity to the changes in cell resistance.

### 3.4 Response of Zone Currents and Resistances to Anodic Effects

The control system currently used effectively manages anodic effects, reducing the effect coefficient to less than 0.1 times per day per cell. However, we fortunately tracked an anodic effect that occurred in the measurement cell at 8:15 on May 16th. Figure 6 shows the changes in zone currents and resistances during the effect. For ease of description, we start timing from 8:13, setting it as 0 seconds, to observe the response characteristics of anode currents and resistances in the six zones.

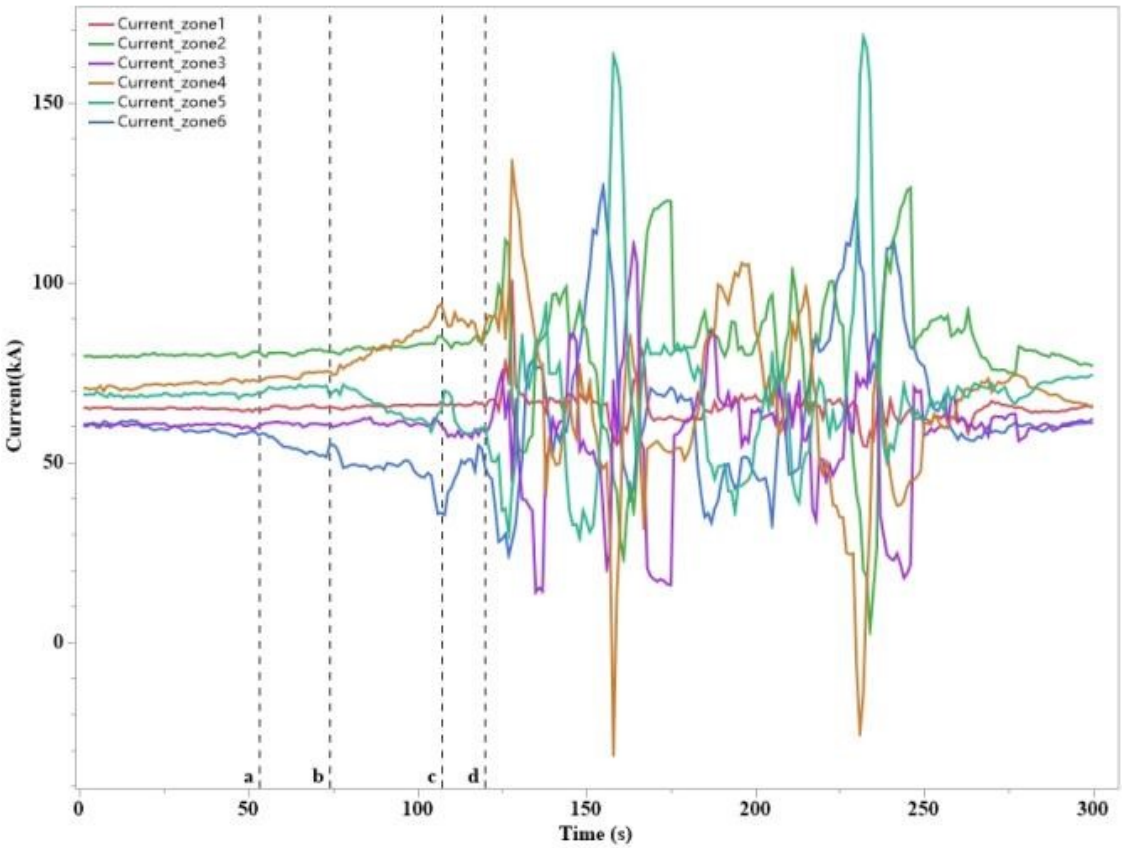


**Figure 6a. The changes in zone currents during an anodic effect that occurred in the measurement cell at 8:15 on May 16th, setting 8:13 as 0 seconds for ease of description.**

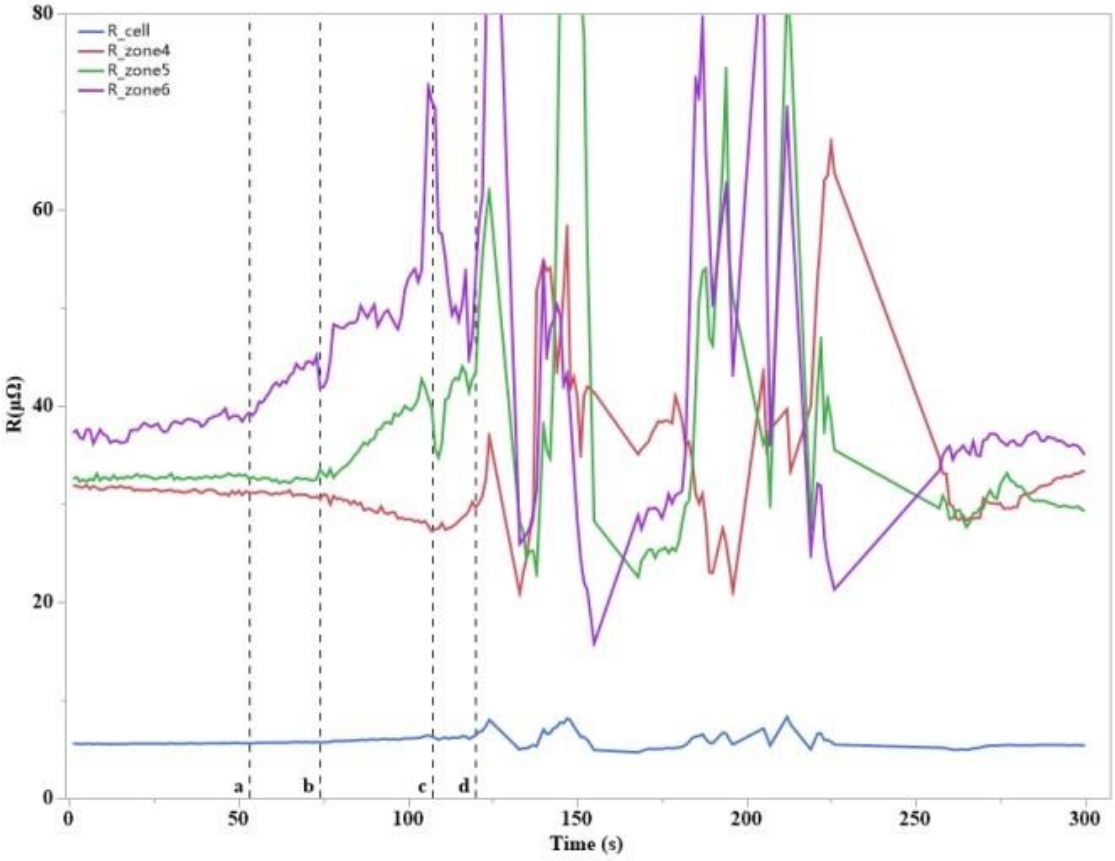


**Figure 6b. The changes in resistances during an anodic effect that occurred in the measurement cell at 8:15 on May 16th, setting 8:13 as 0 seconds for ease of description.**

As seen from Figure 6(a), the anodic effect fully occurred at 122s (dashed line d), but the current changes in each zone varied before that. The current in Zone 6 began to decrease noticeably at 52s (dashed line a). By the time it reached 74s (dashed line b), the current in Zone 5 also diminished, while the current in Zone 4 increased significantly, apparently carrying the reduced current from Zones 6 and 5. At 107 s (dashed line c), Zone 6's current experienced a distinct trough before increasing, which correspondingly caused a concurrent peak in the currents of Zones 5 and 4, followed by a decrease. At 122 s (dashed line d), the currents in the other three zones rapidly increased, marking the occurrence of a full-cell effect.

The zone current effect curves in Figure 6(a) indicate that the onset of the anodic effect follows a gradual process: the effect first occurs in some individual zones, then spreads to other zones, and finally triggers a full-cell effect in an "avalanche" manner. This characteristic is similar to the response of the anodic effect on single anode currents [30] and suggests that real-time monitoring of zone currents could potentially predict and facilitate timely management of full-cell anodic effects.

We observe that when the current in Zone 6 decreases noticeably, there is a clear upward trend in the cell voltage curve. Figure 6(b) shows the corresponding changes in cell resistance. As evident from the figure, by combining the decreasing trend in zone current with the increasing trend in cell voltage, the obtained zone resistance amplifies this effect. The resistances of Zones 5 and 4 also reflect corresponding changes. For comparison, Figure 6(b) also presents the variation in cell resistance, which shows almost no precursor signs of any effect on the same scale. However, zone resistance provided a clear indication about 70 seconds before the effect occurred, which is adequate time for industrial applications. Nevertheless, due to various factors that can influence

zone resistance in practical processes, a large number of examples are still needed to establish the comprehensive patterns of variation for specific applications.

Finally, it's worth noting that in Figure 6(a), we observed negative currents of up to nearly 30 kA (indicated by the red dashed line) during the occurrence of the effect. Whether this is an artifact of the measurement method itself or indeed caused by local reverse currents induced by effect oscillations in the electrolytic cell is worth further investigation.

## 4. Conclusions

In this paper, for the first time, we have achieved online measurement of zone anode currents in a 400 kA electrolytic cell using optical fiber current sensors. The difference between the sum of zone currents and the potline current is no more than 2000 A, with a relative deviation of less than 0.5 %. Through the analysis of zone currents and resistances, the following conclusions can be drawn.

1. The anode currents of different zones in the electrolytic cell vary dynamically, with the maximum and minimum currents deviating from the average by up to 20 %. This indicates that the existing feeding control method of adding alumina at a constant rate is unsuitable and leads to uneven alumina concentration distribution and lower current efficiency in the electrolytic cell. Localized independent feeding of alumina based on zone demand is necessary to address the uniformity of alumina concentration.

2. The response trend of zone resistances to alumina feeding is similar to that of cell resistance, suggesting that independent control of alumina feeding for each zone can be achieved by referencing the existing feeding control strategy based on cell resistance. Alternatively, the existing simultaneous feeding control strategy for the entire cell can be further optimized by monitoring zone resistances.

3. The anodic effect first occurs in some individual zones and then spreads to other zones and finally the entire cell. Changes in zone currents and resistances can be used to predict the high-voltage anodic effects.

## 5. Acknowledgments

The team sincerely thanks the National Natural Science Foundation of China (Project No. 52374349) for its funding support.

## 6. References

1. Vinko Potocnik and Michel Reverdy, History of Computer Control of Aluminum Reduction Cells, *Light Metals* 2021, 591-599.
2. S. Yang, Z. Zou, J. Li et al, Online Anode Current Signal in Aluminum Reduction Cells: Measurements and Prospects, *JOM*, 2016, 68(2), 623–634.
3. Choon-Jie Wong et al., A Smart Individual Anode Current Measurement System and Its Applications, *Light Metals* 2023, 43-51.
4. Nobuo Urata and James W. Evans, The Determination of Pot Current Distribution by Measuring Magnetic Fields, *Light Metals*, 2010, 473-478.
5. James W. Evans and Nobuo Urata, Wireless and Non-Contacting Measurement of Individual Anode Currents in Hall-Héroult Pots; Experience and Benefits, *Light Metals*, 2012, 939-942.
6. Lukas Dion et al., On-line Monitoring of Individual Anode Currents to Understand and Improve the Process Control at Alouette, *Light Metals* 2015, 723-728.

7. Lukas Dion et al., Preventive Treatment of Anode Effects Using On-Line Individual Anode Current Monitoring, *Light Metals*, 2017, 509-517.
8. Klaus Bohnert et al, Fiber-Optic Current Sensor for Electrowinning of Metals, *Journal of Lightwave Technology*, 2007, 25(11), 3602-3609.
9. Yongliang Wang et al., Testing and Characterization of Anode Current in Aluminum Reduction Cells, *Met Mater Trans B*, 2016, 47, 1986-1998.
10. Vinko Potocnik, Alexander Arkhipov, Nadia Ahli and Abdalla Alzrooni, Measurement of DC Busbar Currents in Aluminium Smelters, P*roceedings of 35th international ICSOBA conference*, 2–5 October 2017, Hamburg, Germany, *Travaux* 46, 1113-1128.
11. Joan Boulanger, Anne Gosselin et al., Imaging Alumina Distribution Using Low-Voltage Anode Effect Detections in Anodic Current, *Light Metals*, 2022, 231-238.
12. Jun Tie, Rentao Zhao, Zhifang Zhang, Wentang Zheng, System and Method for Measuring Anode Current of Aluminum Electrolytic Cell, *US Patent 20200032408A1*, 2020.
13. Xiao H, Tie J, Lei J et al., A System, Method and Electronic Equipment for Measuring Zone Anode Current in an Aluminum Reduction Cell, *Chinese Patent 2023106872489*, 9 June 2023.
14. Tie J, Xiao H, Zhao RT, et al., Zone Anode Current Measurement System and Electrolytic Cell Measurement System Based on Individual Fiber Ring, *Chinese Patent 2023109487869*, 31 July 2023.
15. Yi Meng, Jun Tie, Chun Li, Rentao Zhao, Hongwei Jiang, Xingzu Peng, Hao Xiao, Dongwei Liu, and Jun Lei, Accurate Measurement of Anode Current in Aluminum Electrolysis: From Ideal to Reality, *Light Metals* 2024, 586-595.